

## Polyhedral vesicles: A Brownian dynamics simulation

Hiroshi Noguchi\*

*Department of Theoretical Studies, Institute for Molecular Science, Okazaki 444-8585, Japan*

(Received 10 September 2002; revised manuscript received 5 December 2002; published 2 April 2003)

Polyhedral vesicles with a large bending modulus of the membrane, such as a gel phase lipid membrane, were studied using a Brownian dynamics simulation. The vesicles exhibited various polyhedral morphologies such as tetrahedron and cube shapes. We clarified two types of line defects on the edges of the polyhedrons: cracks of both monolayers at the spontaneous curvature of the monolayer  $C_0 < 0$ , and a crack of the inner monolayer at  $C_0 \geq 0$ . The inner monolayer curved positively around the latter defect. Our results suggest that the polyhedral morphology is controlled by  $C_0$ .

DOI: 10.1103/PhysRevE.67.041901

PACS number(s): 87.16.Dg, 82.70.Uv, 87.16.Ac

### I. INTRODUCTION

Amphiphilic molecules such as lipids and detergents form various structures such as micelles, cylindrical structures, and bilayer membranes in aqueous solution [1,2]. In particular, closed bilayer membranes, i.e., vesicles, are biologically important as model systems for the plasma membrane and intracellular compartments in living cells. Various morphological changes in the vesicles are understood via the Helfrich elastic model [1–5]. However, this model cannot be applied to nonbilayer structures. For example, in an inverted hexagonal  $H_{II}$  phase, the hydrophobic interstice (void) space opens among three cylindrical monolayers. Recently, it is considered that this interstice space is filled by the tilt deformation of amphiphilic molecules, as shown in Fig. 1(a) [6,7]. The molecules tilt with respect to the monolayer surfaces around the junction of the three bilayers. The monolayer surfaces are sharply bent at the junction. The effects of the tilt deformation have also been studied with regard to the fusion intermediates of the fluid phase membranes [8,9].

On the other hand, polyhedral-shaped vesicles of micrometer scale size were observed in a gel phase: a triangular-pyramid or prism-shaped vesicle of a monocomponent lipid [10], and an icosahedral vesicle of mixtures of cationic and anionic surfactants [11]. The membranes are flat on the faces of the polyhedrons and sharply bent at the edges. Since the bending modulus is very large in the gel phase, the polyhedral vesicles would be more stable than the spherical vesicles. The free-energy loss of the defects at the edges would be less than the loss of the constant bending of the membranes in the sphere. Thus, the large bending modulus of the gel phase would be an essential condition for polyhedral vesicles. However, the defect structure at the edges is unresolved. Information on the edge structure is significant to control the morphology of the polyhedral vesicles. These vesicles are expected to be of practical value for drug delivery.

To clarify the edge structure, theories or simulations with molecular resolution are needed. Since molecular dynamics simulations with atomic resolution have only been applied for the  $\sim 10$  ns dynamics of 1000 lipid molecules due to the

restrictions of computational time [12–14], coarse-grained molecular simulations [15–26] have been applied. We studied the fusion and fission dynamics of vesicles using Brownian dynamics [20–23]. The self-assembly into vesicles is simulated by our model [19], a lattice Monte Carlo method [16], and dissipative particle dynamics [25]. However, these simulated vesicles were flexible, and no polyhedral vesicles have been obtained.

In the present paper, we developed our previous model to control the bending modulus of the monolayers by the addition of the curvature potential of a monolayer. Since the regular arrangement of the molecules in the gel phase is not a necessary condition to form a polyhedral vesicle, we used the fluid phase membrane with a large bending modulus. Polyhedral vesicles and two types of defects at the edges, as shown in Figs. 1(b) and 1(c) are obtained. The morphology of the polyhedral vesicles and the defect type depend on the spontaneous curvature of the monolayer,  $C_0$ .

### II. METHOD

An amphiphilic molecule is modeled as rigid rods consisting of one hydrophilic segment ( $j=1$ ) and two hydrophobic segments ( $j=2,3$ ), which are separated by a fixed distance  $\sigma$ . Solvent molecules are not explicitly taken into account, and the “hydrophobic” interaction is mimicked by the multi-body local density potential of the hydrophobic segments. As the details of the basic model were described in our previous papers [19,21], we briefly explain the model here. The motion of the  $j$ th segment of the  $i$ th molecule follows the underdamped Langevin equation with the constraint of a linear molecule. Amphiphilic molecules ( $i=1, \dots, N$ ) interact via

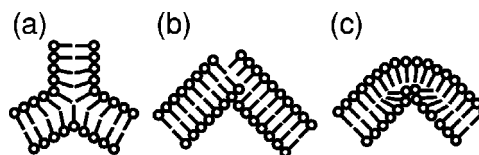


FIG. 1. Three types of line defects. (a) Tilt deformation in the inverted hexagonal phase. (b) Cracks of both monolayers. Hydrophobic segments are partially exposed. (c) Crack of the inner monolayer. Amphiphilic molecules in the inner monolayer tilt with respect to the boundary surfaces of the two monolayers.

\*Electronic mail address: noguchi@ims.ac.jp

a repulsive soft-core potential  $U_{\text{rep}}$ , an attractive hydrophobic potential  $U_{\text{hp}}$ , and a curvature potential  $U_{\text{CV}}$ .

$$U = \sum_{i \neq i'} U_{\text{rep}}(|\mathbf{r}_{i,j} - \mathbf{r}_{i',j'}|) + \sum_{j=2,3} U_{\text{hp}}(\rho_{i,j}) + U_{\text{CV}}, \quad (1)$$

where  $\rho_{i,j}$  is the local density of the hydrophobic segments for the  $j$ th segment of the  $i$ th molecule. Both segments have the same soft radius,  $U_{\text{rep}}(r)/\varepsilon = \exp[-20(r/\sigma - 1)]$ . The hydrophobic interaction is mimicked by the potential  $U_{\text{hp}}(\rho)$ .

$$\rho_{i,j} = \sum_{i \neq i', j'=2,3} h(|\mathbf{r}_{i,j} - \mathbf{r}_{i',j'}|), \quad (2)$$

where

$$h(r) = \frac{1}{\exp\{20(r/\sigma - 1.9)\} + 1}.$$

$\rho_{i,j}$  is the number of hydrophobic segments in the sphere whose radius is  $\approx 1.9\sigma$ .

$$U_{\text{hp}}(\rho)/\varepsilon = \begin{cases} -0.5\rho & (\rho < \rho^* - 1) \\ 0.25(\rho - \rho^*)^2 - c & (\rho^* - 1 \leq \rho < \rho^*) \\ -c & (\rho^* \leq \rho), \end{cases} \quad (3)$$

where  $c$  is given by  $c = 0.5\rho^* - 0.25$ . We used the values  $\rho^* = 10$  and  $14$  at  $j=2$  and  $3$ , respectively. At low density ( $\rho < \rho^* - 1$ ),  $U_{\text{hp}}(\rho)$  acts as the pairwise potential  $-\varepsilon h(r)$ .

To give the bending modulus  $\kappa$  and the spontaneous curvature  $C_0$  of the monolayer membranes, we use the potential  $U_{\text{CV}}$  of the orientational difference of neighboring molecules:

$$U_{\text{CV}} = \sum_{i \neq i'} 0.5\kappa'_{\text{cv}} h(r_{i,i'}) (\mathbf{u}_i - \mathbf{u}_{i'} - C_0 \hat{\mathbf{r}}_{i,i'})^2, \quad (4)$$

where the vector  $\mathbf{u}_i$  is the unit orientational vector of the  $i$ th molecule, and  $\hat{\mathbf{r}}_{i,i'}$  ( $r_{i,i'}$ ) is the unit vector (distance) between the  $i$ th and  $i'$ th molecules:  $\mathbf{u}_i = (\mathbf{r}_{i,1} - \mathbf{r}_{i,3})/|\mathbf{r}_{i,1} - \mathbf{r}_{i,3}|$  and  $\hat{\mathbf{r}}_{i,i'} = (\mathbf{r}_i - \mathbf{r}_{i'})/|\mathbf{r}_i - \mathbf{r}_{i'}|$ , where  $\mathbf{r}_i$  is the center of mass of the  $i$ th molecule. At  $C_0 = 0$ , this potential is similar to the bending elastic potential used in the tethered membrane models [27,28]. When the orientational vectors  $\mathbf{u}_i$  are equal to the normal vectors of the monolayers with no tilt deformation,

$$U_{\text{CV}} = \int 0.5\kappa_{\text{cv}} [(C_1 + C_2 - C_0)^2 - 2C_1C_2 + C_0^2] dA \quad (5)$$

in the continuum limit, where  $C_1$  and  $C_2$  are the two principal curvatures of a monolayer. The spontaneous curvature  $C_0$  is equal to  $C_0' \sigma / \bar{r}_{\text{nb}}$ , where  $\bar{r}_{\text{nb}}$  is the mean distance between neighboring molecules and  $\bar{r}_{\text{nb}} = 1.5\sigma$ . On the assumption of the hexagonal packing of molecules in the monolayers, we obtain  $\kappa_{\text{cv}} = \sqrt{3}\kappa'_{\text{cv}}$ . We used  $\kappa'_{\text{cv}} = 3\varepsilon$  to represent the rigid

membrane, and  $\kappa_{\text{cv}} \approx 5\varepsilon$ . In previous papers, we estimated the bending modulus  $\kappa_0/\varepsilon \approx 0.5$  (half of the bending modulus of bilayers) at  $\kappa'_{\text{cv}} = 0$  [21]. Since  $\kappa_{\text{cv}}$  is tenfold larger than  $\kappa_0$ , the bending elasticity is mainly given by  $U_{\text{CV}}$ , and the bending modulus of the monolayer  $\kappa \approx \kappa_{\text{cv}}$ .

We mainly used the number of molecules  $N = 1000$  and  $k_B T/\varepsilon = 0.2$ , where  $k_B$  is the Boltzmann constant and  $T$  is the temperature. Amphiphilic molecules spontaneously form vesicles in a fluid phase at  $k_B T/\varepsilon = 0.2$  and  $\kappa'_{\text{cv}} = 0$ . The unit length  $\sigma$  corresponds to  $\sim 1$  nm. The unit time step  $\tau_0 = \zeta \sigma^2 / \varepsilon$  corresponds to  $\sim 1$  ns estimated from the lateral diffusion constant of phospholipids at  $30^\circ \text{C}$ ,  $\sim 10^{-7} \text{ cm}^2/\text{s}$  [29,30], where  $\zeta$  is the friction constant of the segments of the molecules. We used three methods to obtain the vesicles at  $\kappa'_{\text{cv}}/\varepsilon = 3$  and  $k_B T/\varepsilon = 0.2$ : quenching, annealing, and  $\kappa_{\text{cv}}$  increasing. In quenching, the simulation starts with spherical vesicles at  $\kappa'_{\text{cv}} = 0$  and the temperature is fixed at  $k_B T/\varepsilon = 0.2$ . In annealing, vesicles are annealed from  $k_B T/\varepsilon = 0.5 - 0.2$ . Temperature decreases with  $k_B T(t)/\varepsilon = (0.3 + a) \exp[\ln[a/(0.3 + a)]t/t_0] + 0.2 - a$ , where  $a = 0.00001$  and  $t_0 = 500000\tau_0$ . In  $\kappa_{\text{cv}}$  increasing, the coefficient  $\kappa'_{\text{cv}}$  linearly increases from  $\kappa'_{\text{cv}}/\varepsilon = 0$  to  $3$  for  $1000000\tau_0$  starting with the spherical vesicles at  $\kappa'_{\text{cv}} = 0$ .

### III. RESULTS AND DISCUSSION

#### A. Morphology of vesicles

Vesicles exhibit various polyhedral morphologies at  $\kappa'_{\text{cv}} = 3\varepsilon$ . The number of faces,  $n_f$ , of a polyhedron increases as  $C_0$  increases. Figure 2 shows examples of the polyhedral vesicles. The edges of the polyhedrons are formed by the line defects [Figs. 1(b) and 1(c)]. The molecules at the line defects are distinguished using the number of neighboring molecules,  $n_i^{\text{nb}}$ , as shown in Fig. 3. The number  $n_i^{\text{nb}}$  is defined as  $n_i^{\text{nb}} = \sum h(r_{i,i'})$ . The inner monolayers are divided into  $n_f$  faces by the defects. At  $C_0 \geq 0$ , the cracks of the inner monolayer [Fig. 1(c)] occur on the edges, and the outer monolayer consists of one curved face [Figs. 2(b) and 2(c)]. At  $C_0 < 0$ , the outer monolayer also exhibits cracks [Fig. 1(b)] on the edges. When the deformation of the left or right side of Fig. 2(a) is formed on the entire circular-line defects, the outer monolayer of the disk-shaped vesicles is divided into three faces (two disks and one cylinder) or two faces, respectively.

Figure 4 shows the mean number of faces,  $\langle n_f \rangle$ , at  $k_B T/\varepsilon = 0.2$  using three methods: quenching, annealing, and  $\kappa_{\text{cv}}$  increasing. The results of annealing are the closest to the equilibrium values. With the other methods, the vesicles are often trapped in metastable states. At  $C_0 > 0$ , vesicles with larger or smaller  $n_f$  values are obtained through quenching or  $\kappa_{\text{cv}}$  increasing, respectively, than through annealing. Thus, the annealing method should be used to obtain regular polyhedrons. It also suggests that polyhedral vesicles with smaller  $n_f$  are formed when  $C_0$  is altered by changes in the solution conditions, such as the salt concentration, after a fluid-gel transition.

Flip-flop motion, which is the transverse motion between the inner and outer monolayers, frequently occurs at  $k_B T/\varepsilon$

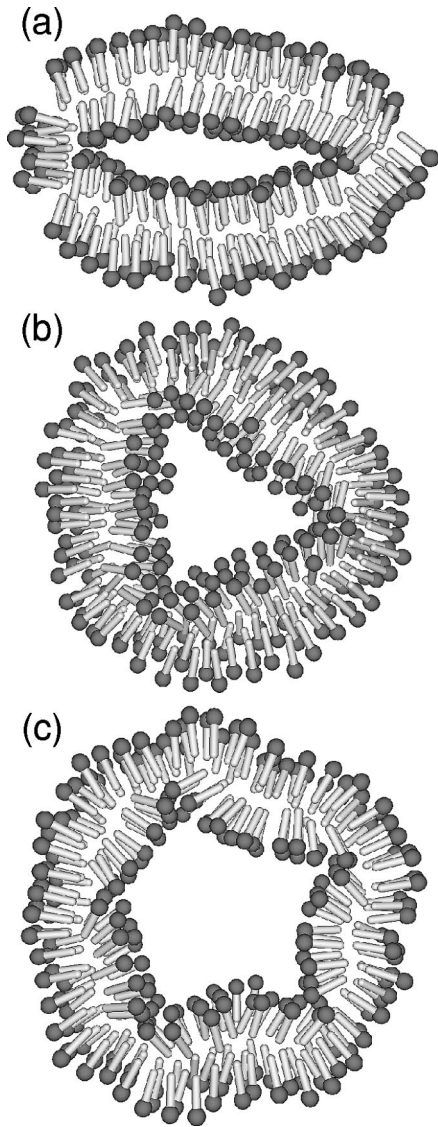


FIG. 2. Sliced snapshots of vesicles at temperature  $k_B T/\epsilon=0.2$  and number of molecules  $N=1000$ . (a) A disk-shaped (dihedral) vesicle at the spontaneous curvature of the monolayer  $C_0\sigma = -0.11$ . (b) A triangular-pyramid shaped (tetrahedral) vesicle at  $C_0\sigma=0.058$ . (c) A pentagonal-prism-shaped (heptahedral) vesicle at  $C_0\sigma=0.23$ . Gray spheres and white cylinders represent hydrophilic and hydrophobic segments of amphiphilic molecules, respectively.

$=0.5$ . The number of molecules in the inner monolayer decreases with an increase in  $n_f$  at  $k_B T/\epsilon=0.5$ , since tilting molecules on the line defects share a larger area. The ratios  $\gamma_{in}$  of the molecules in the inner monolayer are  $0.31(\pm 0.01)$  and  $0.292(\pm 0.003)$  at  $C_0\sigma = -0.11$  ( $n_f=2$ ) and  $C_0\sigma=0.23$  ( $n_f=7.3$ ), respectively. On the other hand, flip-flop motion rarely occurs and the ratio  $\gamma_{in}$  is fixed at  $\gamma_{in}=0.328(\pm 0.003)$  at the fixed temperature  $k_B T/\epsilon=0.2$ . In typical experimental conditions, flip-flop motion is very slow, and the half-life is more than several hours, even in the fluid phase [31,32]. Thus experimentally, the ratio  $\gamma_{in}$  of the polyhedral vesicles should not reach an equilibrium value as well as the simulation at the fixed temperature  $k_B T/\epsilon=0.2$ .

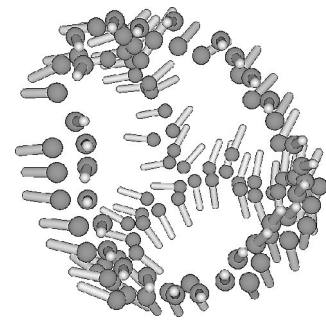


FIG. 3. Line defects (edges) of the tetrahedral vesicle in Fig. 2(b). The snapshot is viewed from the same viewpoint. The molecules with the number of neighboring molecules  $n_i^{nb} < 4.5$  in the inner monolayer are shown.

In the polyhedrons obtained, three edges are connected at any vertex. The connections of more edges are unstable and are not formed. The number of edges,  $n_e$ , then equals 1.5-fold the number of vertices,  $n_v$ , because each edge contacts two vertices. We obtain  $n_e=3(n_f-2)$  and  $n_v=2(n_f-2)$  from this relationship and Euler's formula for a convex polyhedron ( $n_f+n_v-n_e=2$ ). At  $n_f \geq 6$ , multiple types of polyhedrons with the same number of faces exist in this rule. However, we obtained only one or two types of polyhedrons: i.e., cube ( $4^6$ ) at  $n_f=6$ ; pentagonal prism ( $4^5, 5^2$ ) and ( $3^1, 4^3, 5^3$ ) at  $n_f=7$ ; ( $4^4, 5^4$ ) at  $n_f=8$ ; ( $4^3, 5^6$ ) and ( $4^4, 5^4, 6^1$ ) at  $n_f=9$ , where ( $p^q$ ) represents a polyhedron with  $q$   $p$  gons. Thus, polyhedrons with low symmetry or including small faces are not formed very much.

At a large spontaneous curvature,  $C_0\sigma=0.35$  and  $k_B T/\epsilon=0.5$ , a vesicle divides into two or three vesicles as shown in Fig. 5. Some regions of the membrane bend outside with cracks of the outer monolayer, and the membrane is divided at these cracks [Figs. 5(b) and 5(c)]. At  $k_B T/\epsilon=0.2$ , these cracks of the outer monolayer are stable, and vesicles exhibit complex morphologies with concave edges. The morphology of the polyhedral vesicles depends on the size of the vesicles. Vesicles with  $N=2000$  exhibit concave edges even at  $C_0\sigma=0.23$ .

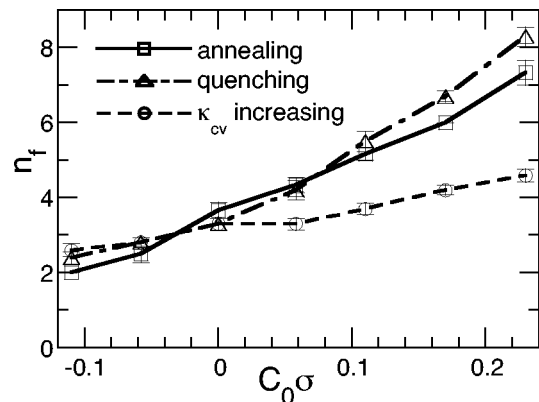


FIG. 4. Spontaneous curvature  $C_0$  dependence of the mean number of faces  $\langle n_f \rangle$  of polyhedrons obtained by three methods at  $N=1000$  and  $k_B T/\epsilon=0.2$ .

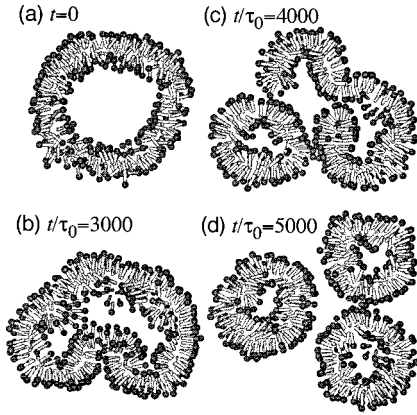


FIG. 5. Sequential sliced snapshots of vesicle fission at  $C_0\sigma = 0.35$ ,  $k_B T/\varepsilon = 0.5$ , and  $N = 1000$ . The initial state is a spherical vesicle at  $\kappa'_{cv}/\varepsilon = 0$  and  $k_B T/\varepsilon = 0.5$ .

### B. Curvature of the membrane

In this section we describe two types of the curvature of monolayer membrane: the curvature (splay) for molecules and the curvature of membrane surface. The difference between these two curvatures is caused by the tilt deformation [7]. Figure 6(a) shows the  $C_0$  dependence of the curvatures of four polyhedrons at  $C_0 \geq 0$ , where  $C_{am}$  is the curvature (splay) for amphiphilic molecules,  $\langle C_{am} \rangle \bar{r}_{nb} = [\sum (\mathbf{u}_i - \mathbf{u}_{i'}) \hat{\mathbf{r}}_{i,i'} h(r_{i,i'})] / [\sum h(r_{i,i'})]$ . The mean curvature  $\langle C_{am}^{out} \rangle$  of the outer monolayer is almost independent of  $C_0$  and  $n_f$  at  $C_0 \geq 0$ . At  $C_0 < 0$ ,  $\langle C_{am}^{out} \rangle$  decreases because of the cracks of the outer monolayers:  $\langle C_{am}^{out} \rangle \sigma = 0.0325 (\pm 0.0005)$  at  $C_0 \sigma$

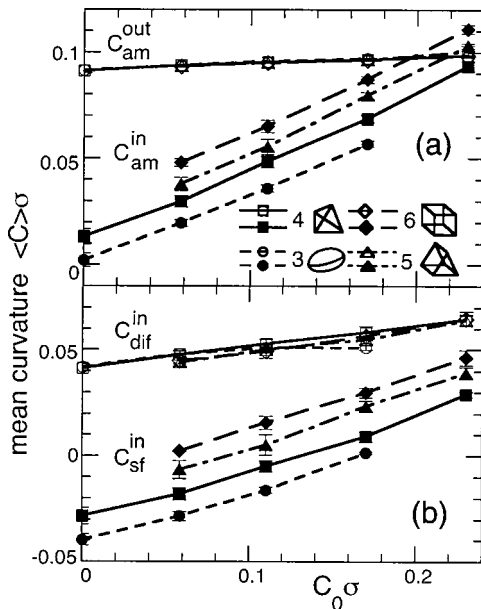


FIG. 6. Spontaneous curvature  $C_0$  dependence of (a) the mean curvature for amphiphilic molecules,  $\langle C_{am} \rangle$  and (b) the mean curvature for the monolayer surface,  $\langle C_{sf} \rangle$ , and the difference,  $\langle C_{dif} \rangle = \langle C_{am} - C_{sf} \rangle$  at  $N = 1000$ ,  $k_B T/\varepsilon = 0.2$ , and  $\gamma_{in} = 0.328 (\pm 0.003)$ . The superscripts “in” and “out” represent the inner and outer monolayers, respectively. Circles: rugby-ball shaped trihedron. Squares: tetrahedron. Triangles: triangular prism. Diamonds: cube.

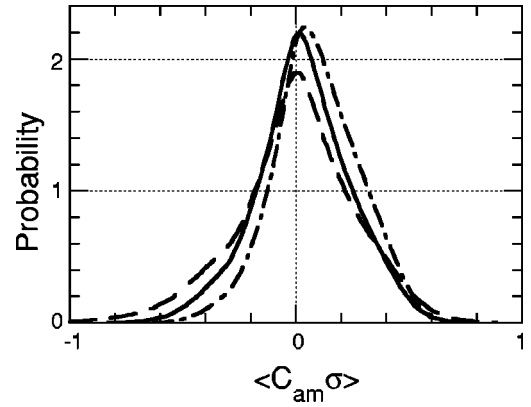


FIG. 7. Probability distribution of the curvatures,  $C_{am}$ , for molecules at  $\kappa'_{cv} = 0$ . Solid line: flat bilayer with 1.11 molecules per  $\sigma^2$ . Broken line: inner monolayer of vesicles with  $N = 1000$ . Broken-and-dotted line: outer monolayer of vesicles with  $N = 1000$ .

$= -0.11$ . On the other hand,  $\langle C_{am}^{in} \rangle$  of the inner monolayer increases with an increase in  $C_0$  and  $n_f$ , since the inner monolayers curve positively around the crack of the inner monolayers. The mean curvature  $\langle C_{am}^{in} \rangle$  for a larger  $n_f$  is closer to  $C_0$ , although more hydrophilic segments contact the hydrophobic segments at the line defects. The curvature  $C_{am}$  does not coincide with the curvature of the monolayers, since molecules can tilt with respect to the monolayer surface. To clarify this tilt, we estimated the curvature  $C_{sf}$  for the monolayer surface,  $\langle C_{sf} \rangle \bar{r}_{nb} = [\sum (\mathbf{n}_i - \mathbf{n}_{i'}) \hat{\mathbf{r}}_{i,i'} h(r_{i,i'})] / [\sum h(r_{i,i'})]$ , where  $\mathbf{n}_i$  is the normal vector of the monolayer surface at  $\mathbf{r}_i$ . We defined  $\mathbf{n}_i$  as the vector minimizing  $\varepsilon_i = \sum h(r_{i,i'}) (\mathbf{n}_i \cdot \hat{\mathbf{r}}_{i,i'})^2$  when  $n_i^{nb} > 2.5$ . This minimizing vector is the eigenvector with the smallest eigenvalue of the moment tensor of inertia of the neighboring molecules. Figure 6(b) shows the curvatures  $\langle C_{sf}^{in} \rangle$  of the inner monolayer surface and the difference  $\langle C_{dif}^{in} \rangle$  between the two curvatures. The inner monolayer surface tilts with respect to the boundary surfaces of the two monolayers, and the molecules in the inner monolayer tilt with respect to the inner monolayer. Both tilts increase  $C_{am}$ . Since the molecular tilt in the inner monolayer,  $\langle C_{dif}^{in} \rangle$ , is almost independent of  $n_f$ , the length of the line defects only changes the curvature  $\langle C_{sf}^{in} \rangle$  of the inner monolayer surface. The length of line defects increases with  $n_f$ . Thus the polyhedral morphology at equilibrium should be determined by the effects of the line defects on  $\langle C_{sf}^{in} \rangle$  and the hydrophobic interaction.

The curvature difference  $C_{dif}$  is also a useful parameter for the flexible membranes. We found that the spontaneous curvature  $C_0$  can be estimated using this tilt deformation with respect to the monolayer surface. The flexible membranes at  $\kappa'_{cv} = 0$  have positive spontaneous curvature induced by the asymmetric attractive interaction. Three segments have the same excluded volume, and the segment of the hydrophobic end,  $j=3$ , has an attractive interaction, although the segment of the hydrophilic end,  $j=1$ , has no attractive interaction. The probability distribution of  $C_{am}$  exhibits an asymmetric shape rather than the Gaussian curve, as shown in Fig. 7. We estimated the effective spontaneous cur-

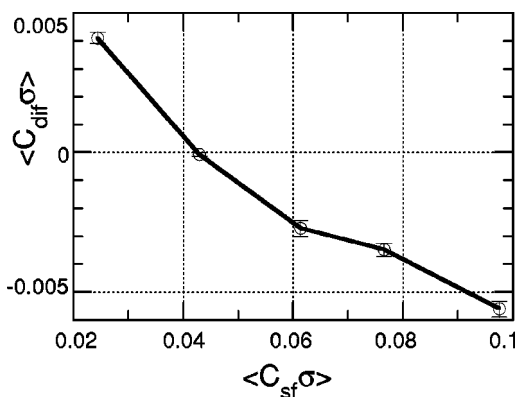


FIG. 8. Curvature of the monolayer surface,  $C_{sf}$ , vs the difference of the two curvatures,  $C_{dif}$ . These values are obtained in the simulations for a flat bilayer, tube-shaped vesicles, and spherical vesicles.

vature  $C_0$  from the  $C_{sf}$  dependence on  $C_{dif}$ , as shown in Fig. 8. At  $C_{sf} < C_0$  or  $C_{sf} > C_0$ , molecules tilt to reduce  $|C_{am} - C_0|$  and  $C_{dif}$  shows a positive or negative value, respectively. Thus, we obtain  $C_0 \sigma \approx 0.04$  at  $\kappa'_{cv} = 0$  and  $k_B T / \varepsilon = 0.2$ .

#### IV. CONCLUSION

We have clarified that a vesicle with a large bending modulus forms polyhedral morphologies. The cracks of the inner or both monolayers are formed on the edges of the polyhedrons. The face number  $n_f$  of the polyhedron increases with  $C_0$ . At a large spontaneous curvature, a vesicle divides into smaller vesicles. In the polyhedral vesicles, molecules

tilt with respect to the monolayer surfaces to reduce the curvature energy. The effective spontaneous curvature of a membrane can be estimated using this tilt deformation.

The line defects may be interpreted using the correction terms of the Helfrich model, the local minimum at a large  $C_1 + C_2$ . The morphology of the polyhedral vesicles may then be obtained from the Euler-Lagrange differential equation. Similar deformations to the crack of the inner monolayer are seen in our daily experience. When a rubber hose is strongly bent, one side of the hose becomes hollow and the other side bends smoothly.

The morphology of polyhedral vesicles depends on the properties of the molecules. The regular arrangement of molecules in gel phase membranes affects the morphology. The hexagonal packing of molecules should stabilize the triangular and hexagonal faces. The simulation results suggest that polyhedral vesicles are experimentally formed even in the fluid phase when the bending modulus is sufficiently large. The stability of the cracks is dependent on its atomic structure. Molecular simulations with atomic resolution are expected to solve the crack structure of lipid membranes. In some multicomponent vesicles, phase separation occurs at the edges or vertices of the polyhedrons. Dubois *et al.* reported that the segregated anionic surfactants form pores at the vertices [11]. Various polyhedral vesicles are likely to be experimentally observed under the control of  $C_0$  and other conditions.

#### ACKNOWLEDGMENTS

This work was supported in part by a Grant-in-Aid for Scientific Research from the Ministry of Education, Culture, Sports, Science, and Technology of Japan.

- 
- [1] *Structure and Dynamics of Membranes*, edited by R. Lipowsky and E. Sackmann (Elsevier Science, Amsterdam, 1995).
- [2] S.A. Safran, *Statistical Thermodynamics of Surfaces, Interfaces, and Membranes* (Addison-Wesley, New York, 1994).
- [3] W. Helfrich, *Z. Naturforsch. C* **28**, 693 (1973).
- [4] U. Seifert, *Adv. Phys.* **46**, 13 (1997).
- [5] H. Hotani, F. Nomura, and Y. Suzuki, *Curr. Opin. Colloid Interface Sci.* **4**, 358 (1999).
- [6] M. Hamm and M.M. Kozlov, *Eur. Phys. J. B* **6**, 519 (1998).
- [7] M. Hamm and M.M. Kozlov, *Eur. Phys. J. E* **3**, 323 (2000).
- [8] P.I. Kuzmin, J. Zimmerberg, Yu.A. Chizmadzhev, and F.S. Cohen, *Proc. Natl. Acad. Sci. U.S.A.* **98**, 7235 (2001).
- [9] Y. Kozlovsky and M.M. Kozlov, *Biophys. J.* **82**, 882 (2002).
- [10] E. Sackmann, *FEBS Lett.* **346**, 3 (1994).
- [11] M. Dubois *et al.*, *Nature (London)* **411**, 672 (2001).
- [12] L.R. Forrest and M.S.P. Sansom, *Curr. Opin. Struct. Biol.* **10**, 174 (2000).
- [13] S.E. Feller, *Curr. Opin. Colloid Interface Sci.* **5**, 217 (2000).
- [14] S.J. Marrink, E. Lindahl, O. Edholm, and A.E. Mark, *J. Am. Chem. Soc.* **123**, 8638 (2001).
- [15] S. Karaborni *et al.*, *Science* **266**, 254 (1994).
- [16] A.T. Bernardes, *J. Phys. II* **6**, 169 (1996).
- [17] R. Goetz, G. Gompper, and R. Lipowsky, *Phys. Rev. Lett.* **82**, 221 (1999).
- [18] T. Soddemann, B. Dünweg, and K. Kremer, *Eur. Phys. J. E* **6**, 409 (2001).
- [19] H. Noguchi and M. Takasu, *Phys. Rev. E* **64**, 041913 (2001).
- [20] H. Noguchi and M. Takasu, *J. Chem. Phys.* **115**, 9547 (2001).
- [21] H. Noguchi and M. Takasu, *Biophys. J.* **83**, 299 (2002).
- [22] H. Noguchi and M. Takasu, *Phys. Rev. E* **65**, 051907 (2002).
- [23] H. Noguchi, *J. Chem. Phys.* **117**, 8130 (2002).
- [24] R.D. Groot and K.L. Rabone, *Biophys. J.* **81**, 725 (2001).
- [25] S. Yamamoto, Y. Maruyama, and S.-a. Hyodo, *J. Chem. Phys.* **116**, 5842 (2002).
- [26] J.C. Shillcock and R. Lipowsky, *J. Chem. Phys.* **117**, 5048 (2002).
- [27] H.S. Seung and D.R. Nelson, *Phys. Rev. A* **38**, 1005 (1988).
- [28] G. Gompper and D.M. Kroll, *Phys. Rev. E* **51**, 514 (1995).
- [29] E.-S. Wu, K. Jacobson, and D. Papahadjopoulos, *Biochemistry* **16**, 3936 (1977).
- [30] W. Pfeiffer *et al.*, *Europhys. Lett.* **8**, 201 (1989).
- [31] R.D. Kornberg and H.M. McConnell, *Biochemistry* **10**, 1111 (1971).
- [32] P.F. Devaux, *Biochemistry* **30**, 1163 (1991).